Investigation of Directional Filter on Kube-Pentland's 3D Surface Reflectance Model using Photometric Stereo

Jiahua Wu
Silsoe Research Institute
Wrest Park, Silsoe
Beds, MK45 4HS
United Kingdom
jerry.wu@bbsrc.ac.uk

Mike J Chantler
School of Mathematical and Computer Sciences
Heriot-Watt University, Edinburgh,
EH14 4AS
United Kingdom
m.j.chantler@hw.ac.uk

Abstract

This paper uses theory, simulation and laboratory experiment to investigate the directional filter on Kube and Pentland's linear reflectance model which presents the image directionality as a product of the illuminant direction and surface directionality. As a result, a surface rotation is not equivalent to an image rotation if the illuminant is not rotated. It can be seen that the directional filter characteristics of an image are described by the term of cosine function. The non-linear and shadowing effects neglected by the model are also investigated. Finally surface orientations estimated from this model using photometric stereo are examined, and experimental results verify the theoretical predictions.

Keywords: 3D surface, directional filter, illumination, photometric stereo, reflectance model, texture.

1 Introduction

Many texture features have been presented that are invariant to image rotation [1] [2] [3]. They normally derive their features directly from a single image and are tested using rotated images. However, in many cases rotation of a 3D textured surface produces images that differ radically from those provided by pure image rotation (see Figure 1). These images show that rotation of a 3D surface texture does not result in a simple rotation of the image texture. This is mainly due to the directional filtering effect of imaging using side-lighting [4] [5]. Such changes in appearance can cause significant failures in image-base texture classifiers [5].

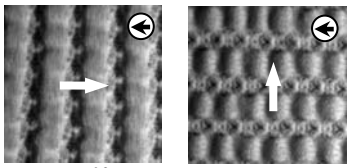

Figure 1: Two images of the same directional 3D rotated surface texture with identical illuminant. The surface has been rotated through of 0^o and 90^o (indicated by the white arrows in the centre). The illuminant tilt defined in Figure 2 is kept constant at $\tau=0°$ (indicated by the black arrows in white circles).

Few take into account these problems. Exceptions include Leung and Malik's classification system which used the images obtained under 20 different illumination and orientation conditions [6]; Nayer and Dana who developed histogram and correlation models of 3D surface textures by using CUReT database [7]; Dana *et al.* developed BTF (Bi-directional Texture Function) database which described the appearance of a textured surface as a function of the illumination and viewing directions [8], and Chantler and Wu presented approaches that used 1D and 2D spectrum of surface gradient and albedo data estimated using photometric stereo [9] [10].

In this paper, we investigate the directional filter on Kube and Pentland's reflectance model [11] which predicts that the intensity approximates a linear combination of the surface derivatives. In the model, the image directionality is a product of the illuminant direction and surface directionality. As a result, a surface rotation is not equivalent to an image rotation if the illuminant is not rotated. It also can be seen that the directional filter characteristics of an image are described by the term of cosine function. The non-linear and shadowing effects neglected by the Kube and Pentland's model are considered too. Finally we extract surface orientations based on this model using photometric stereo, and experimental results verify the theoretical predictions.

2 Kube and Pentland's Reflectance Model for 3D Surface

2.1 Imaging Geometry

Kube and Pentland [11] present a spectral model for the formation of the image from an illuminated fractal surface. The imaging geometry assumptions (see

Figure 2) are as follows: the test surface is mounted in the *x*-*y* plane and is perpendicular to the camera axis (the *z*-axis); the test surface is illuminated by a point source located at infinity, *i.e.* the incident vector field is uniform in magnitude and direction over the test area; the tilt angle τ of illumination is the angle that the projection of the illuminant vector incident onto the test surface plane makes with an axis in that plane; the slant angle σ is the angle that the illuminant vector makes with a normal to the test surface plane; surface rotation is measured in the *x*-*y* plane; orthographic camera model assumed.

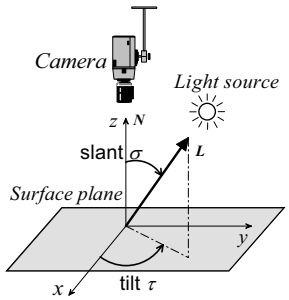

Figure 2: Imaging geometry.

2.2 Linear Reflectance Model

We assume a Lambertain reflectance function. This can be expressed in terms of the partial derivatives of the surface height function:

$$i(x,y)=\rho(x,y)\left(\frac{-p(x,y)\cos\tau\sin\sigma-q(x,y)\sin\tau\sin\sigma+\cos\sigma}{\sqrt{p^2(x,y)+q^2(x,y)+1}}\right) \quad (1)$$

Where σ, τ are the illuminant's slant and tilt angles, $\rho(x,y)$ is the albedo of the surface, and the partial derivatives are as defined below:

$$p(x,y)=\partial z/\partial x \quad (2)$$

$$q(x,y)=\partial z/\partial y \quad (3)$$

This results in a non-linear operation at each facet. Therefore taking the MacLaurin expansion of $1/\sqrt{p^2+q^2+1}$ in the equation (1), where $\rho(x,y)=1$ and yielding

$$i(x,y)=\left(-p\cos\tau\sin\sigma-q\sin\tau\sin\sigma+\cos\sigma\right)\left[1-\frac{p^2+q^2}{2!}+\frac{9\left(p^2+q^2\right)^2}{4!}\ldots\right] \quad (4)$$

Using the first three terms it forms a linear estimation:

$$i(x,y)=-p\cos\tau\sin\sigma-q\sin\tau\sin\sigma+\cos\sigma \quad (5)$$

where the approximation is reasonable at $p>>p^2$ and $q>>q^2$ (*i.e.* p and q are small) so that the quadratic and higher order terms can be neglected [4].

2.3 Frequency Domain Responses

We note that since differentiation is a linear operation, equation (5) can be transformed into the frequency domain and expressed as a function of the surface magnitude spectrum while discarding the constant term:

$$I_m(\omega,\theta)=i.\omega.\sin\sigma.\cos(\theta-\tau).S_m(\omega,\theta) \quad (6)$$

where $I_m(\omega,\theta)$ is the image magnitude spectrum; $S_m(\omega,\theta)$ is the surface magnitude spectrum; ω is the angular frequency of the Fourier component; θ is its direction with respect to the *x*-axis; and *i* represents a $90°$ phase shift.

This equation can be divided into three components:

1. surface response $I_{ms}(\omega,\theta)=\left[i\cdot\omega\cdot S_m(\omega,\theta)\right]$;

2. tilt response $I_{m\tau}(\omega,\theta)=\left[\cos(\theta-\tau)\right]$; and

3. slant response $I_{m\sigma}(\omega,\theta)=\left[\sin\sigma\right]$.

In this paper it is more helpful to express equation (6) in terms of its power spectrum:

$$I(\omega,\theta)=\omega^2\left|\sin\sigma\right|^2\left|\cos(\theta-\tau)\right|^2 S_\varphi(\omega,\theta) \quad (7)$$

where (ω,θ) is the polar form of spatial frequency with $\theta=0°$ being the direction of the *x*-axis; $I(\omega,\theta)$ is the image power spectrum, and $S_\varphi(\omega,\theta)$ is the surface power spectrum of a surface orientated at φ.

This equation contains simple trigonometric terms, which enable the directional effect of illumination to be more easily understood. Since we are interested in surface rotation, we only deal with the effects of the $\left|\cos(\theta-\sigma)\right|^2$ term, which is a directional filter and is independent of radial frequency ω.

2.4 Directional Filter

2.4.1 Illumination Directional Filter

In equation (6), the most important feature of Kube and Pentland's model is the term $I_{m\tau}(\omega,\theta)=\left[\cos(\theta-\tau)\right]$, which predicts the effect of illumination directional filter. This can be understood by considering Figure 3.

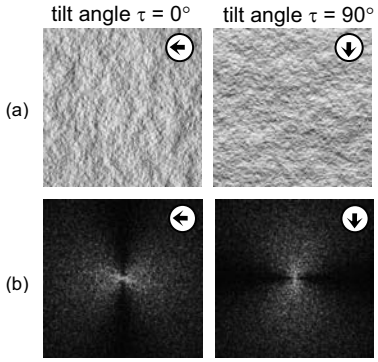

Figure 3: A fractal surface rendered by Kube and Pentland's model (a). surfaces at two different illumination directions (indicated by the black arrows in white circles); (b). their power spectral densities.

We may see that, for an isotropic surface, image directionality is only due to the directional effect of the illuminant. Therefore, changing the illuminant directions causes a change in the direction of energy in the corresponding power spectral density. Furthermore, the highest texture energy lies in the direction of the illuminant tilt angle τ.

2.4.2 Image Variance is Not a Surface Rotation Invariant Feature for Directional 3D Surfaces

- *Theory*

With regard to the equation (7), the image variance is the integral of the image power spectrum, assuming the mean component to be equal to zero. The following can therefore be obtained:

$$\sigma^2(\varphi) = \int_0^{\infty} \omega^2 \sin^2(\sigma) \cdot 2 \int_0^{\pi} \cos^2(\theta - \tau) \cdot S_{\varphi}(\omega, \theta)\, d\theta\, d\omega \tag{8}$$

If we consider a new axis with the direction of the unidirectional surface texture where $\theta^* = \theta - \varphi$, and then equation (8) becomes:

$$\sigma^2(\varphi) = \int_0^{\infty} \omega^2 \sin^2(\sigma) \cdot 2 \int_{-\varphi}^{\pi-\varphi} \cos^2(\theta^* + \varphi - \tau) \cdot S_{\varphi}(\omega, \theta^*)\, d\theta^*\, d\omega \tag{9}$$

Now if the inner integral part of the equation (9) is taken into account

$$\begin{aligned}
&2 \int_{-\varphi}^{\pi-\varphi} \cos^2(\theta^* + \varphi - \tau) \cdot S_{\varphi}(\omega, \theta^*)\, d\theta^* \\
&= \int_0^{\pi} \left[1 + \cos(2\theta^* + 2\varphi - 2\tau)\right] \cdot S_{\varphi}(\omega, \theta^*)\, d\theta^* \\
&= \int_0^{\pi} S_{\varphi}(\omega, \theta^*)\, d\theta^* + \int_0^{\pi} \cos(2\theta^* + 2\varphi - 2\tau) \cdot S_{\varphi}(\omega, \theta^*)\, d\theta^* \\
&= \int_0^{\pi} S_{\varphi}(\omega, \theta)\, d\theta \\
&\quad + \int_0^{\pi} \left[\cos 2\theta \cdot \cos(2\tau - 2\varphi) + \sin 2\theta \cdot \sin(2\tau - 2\varphi)\right] \cdot S_{\varphi}(\omega, \theta)\, d\theta
\end{aligned} \tag{10}$$

Therefore equation (8) can be simply expressed in the form of

$$\begin{aligned}
\sigma^2(\varphi) &= A + \left[B \cos(2\tau - 2\varphi)\right] + \left[C \sin(2\tau - 2\varphi)\right] \\
&= A + \left[D \cos(2\tau + \phi)\right]
\end{aligned} \tag{11}$$

Where

$$A = \sin^2(\sigma) \int_0^{\infty} \omega^2 \int_0^{\pi} S_{\varphi}(\omega, \theta)\, d\theta\, d\omega$$

$$B = \sin^2(\sigma) \int_0^{\infty} \omega^2 \int_0^{\pi} \cos 2\theta \cdot S_{\varphi}(\omega, \theta)\, d\theta\, d\omega$$

$$C = \sin^2(\sigma) \int_0^{\infty} \omega^2 \int_0^{\pi} \sin 2\theta \cdot S_{\varphi}(\omega, \theta)\, d\theta\, d\omega$$

$$D = \sqrt{B^2 + C^2}$$

$$\phi = \left[\arctan(C / B)\right] + 2\varphi$$

From equation (11), we may note that for an *isotropic surface*, the term *D* will be equal to zero, and then the image variance $\sigma^2(\varphi)$ will be kept constant; on the other hand, for a *directional surface*, the term *D* will not be equal to zero and therefore image variance $\sigma^2(\varphi)$ will be a raised cosine function of surface orientation.

- *Experimental verification*

Figure 5 illustrates the variation of image intensity variance with surface rotation for an isotropic surface *"gr2"* and a directional surface *"wv2"* (shown in Figure 4). We may note that the variance of image intensity for the directional surface *"wv2"* is certainly not invariant to surface rotation and indeed it is following the cosine term predicted in the model by equation (11). It is this directional filter effect that makes the outputs of texture features vary with the orientation of a directional surface.

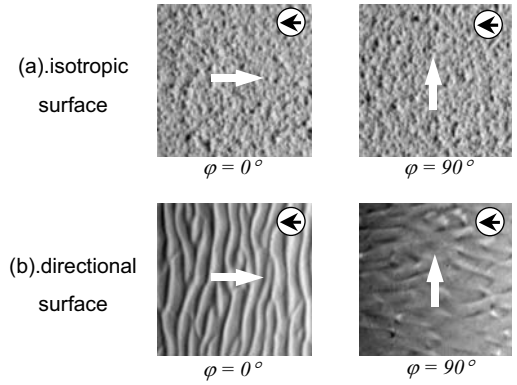

Figure 4: Isotropic surface "gr2" and directional surface "wv2" with rotation φ=0° and 90° (indicated by the white arrows in the centre). The illuminant tilt is kept constant at τ=0° (indicated by the black arrows in white circles).

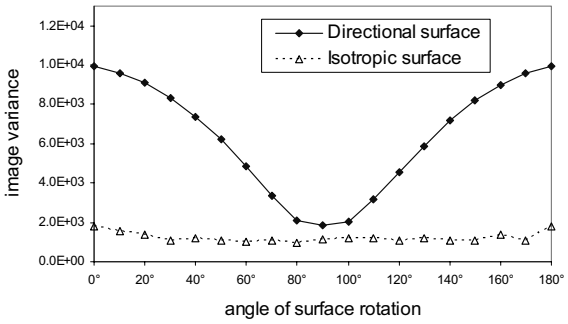

Figure 5: The variation of image intensity variance with surface rotation for an isotropic surface "gr2" and a directional surface "wv2".

- *Surface rotation classification vs. image rotation classification*

An example of classification accuracy for image rotation and surface rotation is given in Figure 6. The statistical classifier is used on a set of isotropic Gabor filters where the features contain no information about the directionality of the texture so that they are

rotation insensitive features. The detailed structure of the rotation insensitive classifier is illustrated in [4].

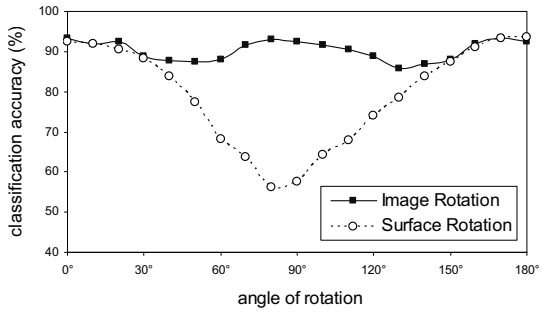

Figure 6: Classification accuracy for image rotation and surface rotation.

2.5 Non-linear Effects

In this section, we investigate the non-linear effects occurring in Kube and Pentland's image model. One of the reasons for this effect, is that the quadratic and higher order terms in equation (4) are neglected in developing the linear image model in equation (5). Furthermore, the linear image model is based on the assumption that surface height variance is low (*i.e.* surface slope is less than *15°* so that $p>>p^2$ and $q>>q^2$) and that the slant angle does not approach *0°*. These assumptions are necessary to allow the Lambertian model to be linearised. Another non-linear contribution is shadowing.

2.5.1 Surface Amplitude Variance

The linear image model assumes a linear relationship between the image variance and surface variance in equation (6). Figure 7 and Figure 8 show the effect of increasing the amplitude of a simple sinusoidal surface on images modelled with perfect Lambertian reflection in equation (1) and linear Lambertian reflection given by Kube and Pentlend's model in equation (5). In order to investigate the effect of the non-linear components, we set the illumination slant angle σ*=45°*. This angle was chosen because the reflection model assumes a $\cos^2$ relationship between slant angle σ and the reflected intensity, and the model seems to be most linear for a slant angle of around *45°*.

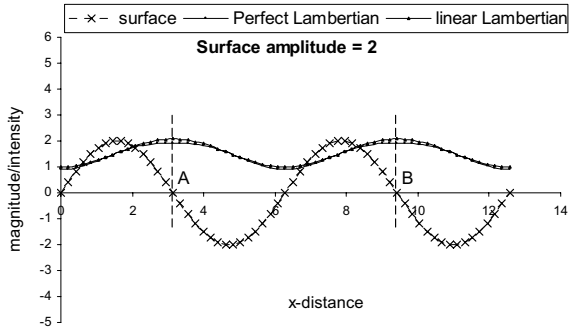

Figure 7: The non-linear effects of a sinusoidal corrugated surface intensity with amplitude=*2*.

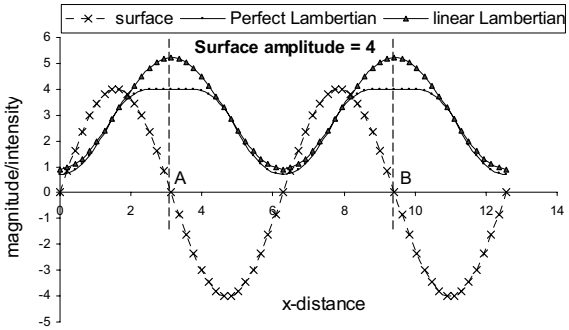

Figure 8: The non-linear effects of a sinusoidal corrugated surface intensity with amplitude=*4*.

In both Figure 7 and Figure 8, it can be seen that the difference or distortion between perfect Lambertian surface and a linear Lambertian surface occurs at the position where the non-linear effects are significant, *i.e.* where the surface slope angles approach their maximum values (the position A and B on the figures). In addition, increasing the surface amplitude from *2* to *4* accentuates these differences.

2.5.2 Clipping

If the slant angle σ is increased, the reflected intensity of the surface becomes further saturated by distortion as it approaches *90°*. This effect can be seen in Figure 9. We may see that the clipping effects apparently become more severe with increasing the slant angle σ, demonstrating the non-linearity in that region.

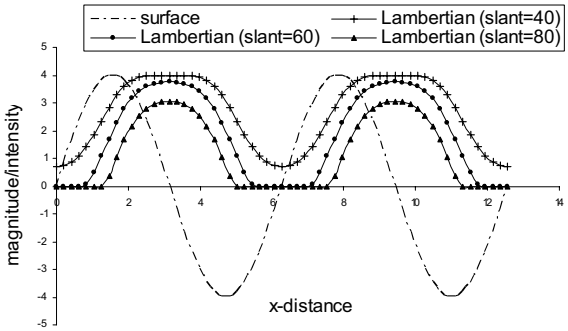

Figure 9: Clipping effect of a sinusoidal corrugated surface illuminated at slant angle σ*=40°*, *60°* and *80°*.

2.5.3 Shadowing

One assumption used in equation (1) is Lambertian reflection where shadowing is ignored. Unfortunately in the real world shadows occur. For a real rough surface, it is acknowledged that there are significant departures from Lambert's law [8] [11]. Moreover, the departures are most marked for specific viewer and light source directions. The Lambertian model breaks down substantially when the angle between the view vector and the surface normal exceeds *60°* [4].

- *Imaging model rendered by the effect of shadow*

In Figure 10, we simulate sinusoidal surfaces rendered by Kube and Pentland's model with shadow.

An approximation to shadowing can be simply modelled in the following way: where the shadow occurs the reflected intensity is clipped and set to *0*. We may clearly see that the distortions caused by the shadowing become more distinctive compared to that without the shadowing effect.

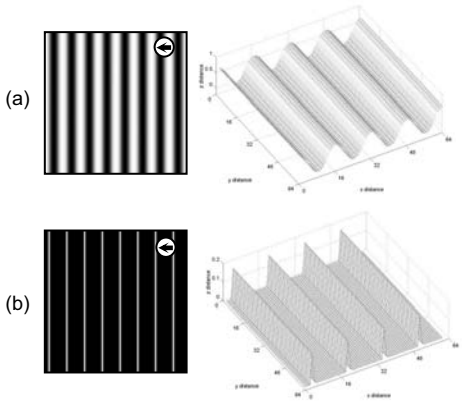

Figure 10: Sinusoidal surfaces rendered by Kube and Pentland's model (tilt angle $\tau=0°$ and slant angle $\sigma=70°$) (a). without any shadow; (b). with shadow.

- *Directional filtering effect reduces with the decrease in the slant angle (σ)*

As discussed in section 2.4, we may note that for a slant angle σ decreasing to near *0°*, the effect of the linear term is reduced compared with that of the square or higher terms. Furthermore the directional filtering effect will be attenuated. Figure 11 shows the effect of decreasing the slant angle σ from *70°* to *10°*. It is apparent that the directional filtering effect reduces as the slant angle σ approaches *0°*. In addition, if the surface is rendered with the effect of *shadow* in Figure 12, the directional filtering effect with the highest slant angle (*i.e.* $\sigma=70°$) is also be attenuated. In this case, the heavy shadow effects the linear approximation of Kube and Pentland's model, where the majority of the reflected intensity are clipped to *0*.

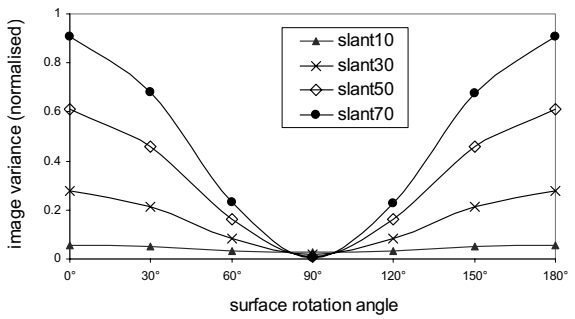

Figure 11: Image intensity variance with surface rotation rendered over a range of illuminant slant angels and *without* any shadow.

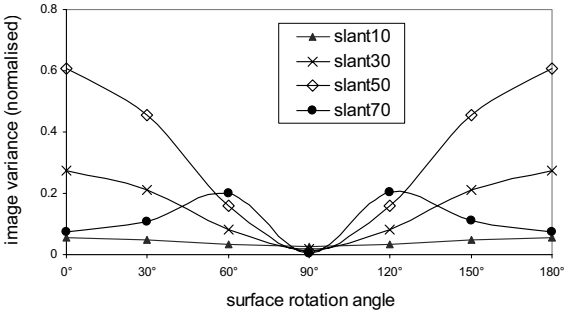

Figure 12: Image intensity variance with surface rotation rendered over a range of illuminant slant angels and *with* shadow.

3 Estimation of 3D Surface Orientation by Photometric Stereo

In the section, we estimate 3D surface orientation from Kube and Pentland's image model by photometric stereo to validate the directional filter effect.

3.1 Three-image Based Photometric Stereo

Three images of the surface are taken under three different illumination conditions to provide three instances of the equation (1). They are used at each *(x,y)* to solve for the three unknowns $\rho(x,y)$, $p(x,y)$, and $q(x,y)$ [12] [4]. Figure 13 shows an example of this process. We note that photometric stereo has the ability to separate surface orientation (p and q) and surface albedo (ρ).

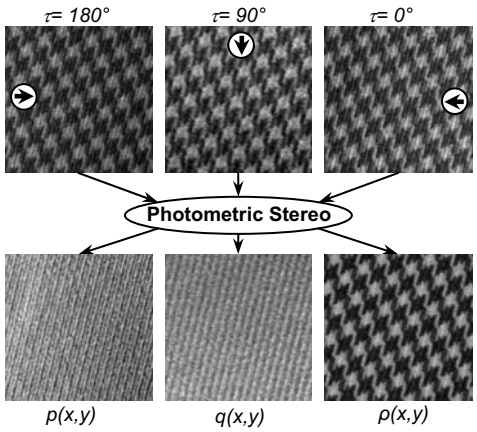

Figure 13: Photometric stereo process. (Note that all surfaces are under the same orientation $\varphi=0°$)

3.2 Presentation of Surface Orientation in Gradient Space

Once the surface properties (p and q) have been captured using photometric stereo, it is useful to represent these data in an alternative form, gradient space $G(p,q)$ which facilitates the mapping of an array of surface normals to a series of co-ordinate points

(p,q) within the 2D gradient space, so that the surface orientation can be estimated [10] [13].

Examples of gradient space *G(p,q)* for texture (shown in Figure 13) at different surface orientations are presented in Figure 14. We can see that the principal axes of gradient space image present the surface orientation (not albedo orientation). We therefore estimate surface orientation by analysing the moment in gradient space [4].

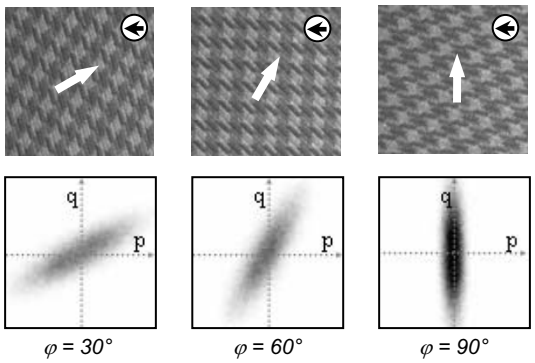

Figure 14: Gradient space *G(p,q)* for 3D surface at different orientations $\varphi = 30°, 60°$ and $90°$ (indicated by the white arrows in the centre). Note that all surfaces are under the constant illumination tilt angles $\tau = 0°$ (indicated by the black arrows in white circles).

Figure 15 shows the estimated surface orientation angles (φ) for above texture surfaces obtained from their corresponding gradient space *G(p,q)* [4]. It can be readily seen that the estimation processing achieves a good result.

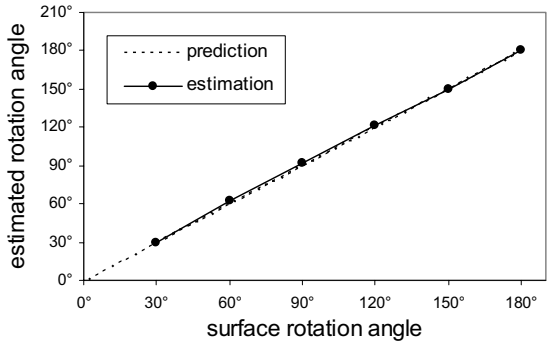

Figure 15: Estimation of surface orientation angles.

4 Conclusions

We have investigated the directional filter on Kube and Pentland's 3D surface linear reflectance model by photometric stereo. The model shows the directional characteristics of image texture are not intrinsic to the physical texture being images, as they are affected by the direction of the illumination. Furthermore behaviours of texture features derived from linear filters can be modelled as a cosine function. Surface orientations estimated from this model using photometric stereo are examined, and experimental results verify the theoretical predictions.

5 References

[1] Cohen, F. S., Fan Z. and Patel, M. A. S., "Classification of rotated and scaled textured images using Gaussian Markov field models", *IEEE Transactions on Pattern Analysis and Machine Intelligence*, Vol.13, pp192-202 (1991).

[2] Porter, R. and Canagarajah, N., "Robust rotaion invariant texture classification: wavelet, Gabor and GMRF based schemes", *IEE Proc. Vision Image Signal Process*, Vol.144, No.3 (1997).

[3] Zhang, J. and Tan, T., "Brief review of invariant texture analysis methods", *Pattern Recognition*, Vol.3, pp735-747 (2002).

[4] Wu, J, "Rotation invariant classification of 3D surface texture using photometric stereo", *PhD Thesis*, Department of Computer Science, Heriot-Watt University, Edinburgh (2003).

[5] Chantler, M. J., "Why illuminant direction is fundamental to texture analysis", *IEE Proc. on Visual Image and Signal Processing*, Vol.142, No.4, pp199-206 (1994).

[6] Leung, T. and Malik, J., "Recognizing surfaces using three-dimensional textons", *Proc. of IEEE International Conference on Computer Vision*, (1999).

[7] Dana, K. J. and Nayar, S. K., "Correlation model for 3D texture", *Proc. of IEEE International Conference on Computer Vision* (1999).

[8] Dana, K. J., Van Ginneken B., Nayar S. K. and Koenderink J. J., "Reflectance and texture of real-world surfaces", *Proc. of IEEE Conference on Computer Vision and Pattern Recognition*, pp151-157 (1997).

[9] Chantler, M. J. and Wu J., "Rotation invariant classification of 3D surface textures using photometric stereo and surface magnitude spectra", *Proc. of British Machine Vision Conference*, Vol.2, pp486-495 (2000).

[10] Wu, J. and Chantler, M. J., "Combining gradient and albedo data for rotation invariant classification of 3D surface texture", *Proc. of International Conference on Computer Vision*, (2003).

[11] Kube, P. and Pentland A., "On the imaging of fractal surfaces", *IEEE Transactions on Pattern Analysis and Machine Intelligence*, Vol.10, No.5, pp704-707 (1988).

[12] Woodham, R., "Photometric method for determining surface orientation from multiple images", *Optical Engineering*, Vol.19, No.1, pp139-144 (1980).

[13] Smith, M. L., "The analysis of surface texture using photometric stereo acquisition and gradient space domain mapping", *Image and Vision Computing*, Vol.17, pp1000-1019 (1999).